Fast Relaxation Dynamics of the Cardiotonic Drug Milrinone in Water Solutions

Maged El-Kemary,† Juan Angel Organero, and Abderrazzak Douhal*

Departamento de Química Física, Sección de Químicas, Facultad de Ciencias del Medio Ambiente, Universidad de Castilla−La Mancha, Avda. Carlos III, S.N., 45071, Toledo, Spain

Received January 2, 2006

The fast relaxation dynamics of 1,6-dihydro-2-methyl-6-oxo-3,4′-bipyridine-5-carbonitrile (milrinone, MIR), a cardiotonic drug, has been characterized in water solutions at different pH. In acidic media, a blue emission reflects a charge-transfer state in the cation (**C**) leading to a more stabilized structure with an emission lifetime of 90 ps. The emission lifetimes of the keto (**K**) and anion (**A**) structures are ∼65 and 310 ps, respectively. Reasons for efficient nonradiative channels are discussed in terms of hydrogen-bonding interactions, intramolecular charge transfer (ICT), and twisting motion. A blue nanosecond-emission observed in almost all the studied pH range is suggested to be due to relaxed **K** due to an ICT reaction. B3LYP (6-31+G**) calculations showed that, in a water cavity, **K** is more stable than the enol form by 7 kcal/mol, and the ICT may take place within the pyridone moiety. At the physiological pH, the inotropic **K** structure is the dominant species (∼100%).

Introduction

1,6-Dihydro-2-methyl-6-oxo-3,4′-bipyridine-5-carbonitrile or milrinone (Chart 1, MIR), a cardiotonic drug, is an inotropic agent (inotropic effects are those that change the strength of contraction of the heart) used for the short-term intravenous therapy of congestive heart failure.[1] MIR in water is known to undergo tautomeric interconversion between keto and enol forms in the ground state through proton transfer with water molecules.[2,3] For pyridin-2(1*H*)-one derivatives, having structures comparable to that of MIR, there is strong experimental and theoretical evidence to prove the dominance of the keto form in aqueous solutions and of the enol structure in gas phase and in nonpolar solvents.[2−6] The dominance of keto species in the ground state of pyridin-2(1*H*)-one in water involves a barrier of ∼35 kcal/mol for the ground-state pathway.[6] Moreover, the electron-donating methyl substitutent of MIR drives the equilibrium toward the keto form in water.[3,7,8] In acidic media a detection of the cation (**C**) species in the ground state of sulfur analogues of MIR has been reported.[9] Both keto and cation structures are the active forms of MIR inotropic agent.[2,9] Figure 1 shows possible tautomeric forms and conformational equilibria in the ground state of MIR in aqueous solutions. Therefore, the inotropic activity of MIR is strongly related to the kind and degree of interaction with water molecules. These may lead to other intramolecular processes involving for example pyridine moiety rotation or orbitals' interaction giving rise to an intramolecular charge-transfer (ICT) reaction. Strong H-bonding interactions of the functional groups of MIR with water molecules may cause the system to evolve to a unique structure: cation, anion, or keto species (Chart 1 and Figure 1). Recently, we have shown the role of twisting motion on the photodynamics of several molecules in solutions and in chemical and biological nanocages.[10−16]

Despite the fact that the photophysics of several drugs have been reported,[17−21] we could not find any report on a photophysical study of MIR. Therefore, in this study, we report on the first fast dynamics of the excited-state population for MIR drug, in aqueous media at different pH. Understanding the fast interaction of the different forms of MIR (anion, cation, and keto) with water molecules may provide a better insight into its inotropic mechanism/activity. The results show the involvement of strong H-bonding interaction with water, ICT, and twisting motion in the photodynamics of MIR.

Chart 1. Molecular Structure of MIR in Its Keto Form[a]

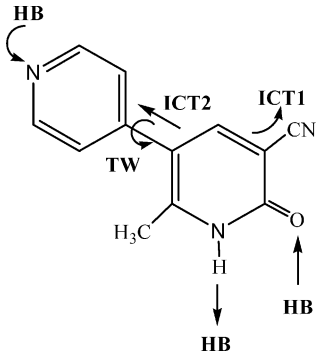

[a] The arrows indicate the possible inter- and intramolecular processes involving H-bonding (HB), charge transfer within the pyridone moiety (ICT1), charge transfer between the two aromatic moities (ICT2), and twisting motion (TW)

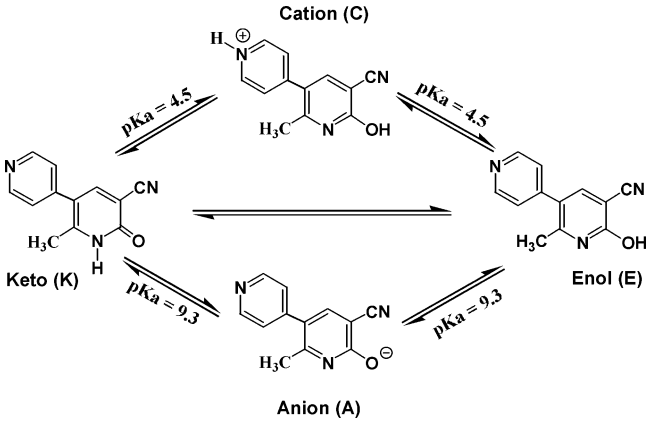

Figure 1. Schematic representation of the possible tautomeric equilibria of MIR at the ground state.

* Corresponding author. Phone: +34-925-265717. Fax: +34-925-268840. E-mail: Abderrazzak.douhal@uclm.es.

† Permanent address: Department of Chemistry, Faculty of Science, Tanta University, 33516 Kafr ElSheikh, Egypt.

10.1021/jm0600038 CCC: $33.50
Published on Web 04/29/2006

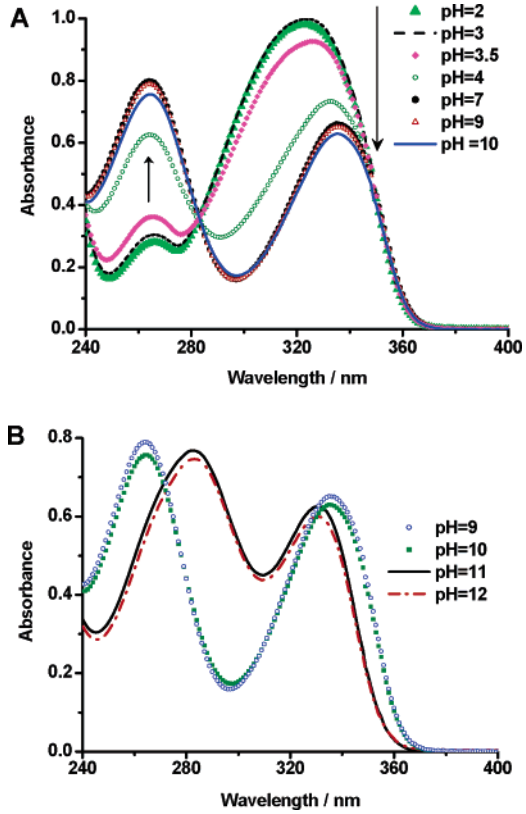

Figure 2. UV−visible absorption spectra of MIR in aqueous solutions at different pH values: (A) pH 2−10 and (B) pH 9−12.

Experimental Section

MIR, purchased from Sigma-Aldrich, was used as received and its purity was checked by thin-layer chromatography (TLC). The pH of the aqueous solutions was adjusted by adding aliquots of HCl or NaOH solutions. Steady-state absorption and emission spectra were recorded on Varian (Cary E1) and Perkin-Elmer (LS 50B) spectrophotometers, respectively. Emission decays were measured by using a time-correlated single-photon counting system (FluoTime 200, PicoQuant). The sample was excited by a 40 ps pulsed (20 MHz) laser centered at 371 nm (PicoQuant), and the emission signal was collected at the magic angle. The IRF of the apparatus was typically 65 ps. The emission decays were fitted to a multiexponential function convoluted with the IRF signal using the Fluofit package (Picoquant). The quality of the fits was characterized in terms of residual distribution and reduced χ^2 value. Details on the apparatus and the procedure of data analysis are described elesewhere.[12] All the measurements were done at 293 ± 1 K.

Theoretical calculations for **K** and **E** of MIR and for 5-methyl-3,4′-bipyridin-6(1*H*)-one (**MB**), a molecule comparable to MIR but without the CN group, were performed with density functional theory using the B3LYP functional and with the 6-31+G** basis set, which includes a set of d polarization functions and a set of diffuse functions on heavy atoms as implemented in the program Gaussian 03.[22−24] The full geometry optimization was carried out by means of the Schlegel gradient optimization algorithm by using redundant internal coordinates. The bulk effect of the solvent (water) was introduced through the isodensity surface-polarized continuum model (IPCM) at S_0 state without reoptimization of the geometries.[24] We have used an electronic density of 0.001 au to define the cavity in this model.

Results and Discussion

Steady-State Absorption and Fluorescence Emission. Figure 2 displays the steady-state UV−visible absorption spectra of MIR in aqueous solutions at different pH. The spectra are separated in two families to show the pH effect on the shapes and position of band maximum. Beginning with pH ∼7 (∼physiological pH), the $S_0 \rightarrow S_1$ lower energy band at ∼336 nm ($\epsilon = 1.68 \times 10^4$ M^{-1} cm^{-1}) and the $S_0 \rightarrow S_2$ higher energy band at 266 nm ($\epsilon = 2 \times 10^4$ M^{-1} cm^{-1}) are due to (π,π^*) transitions.[6] At pH 2−10, two isosbestic points are observed at 283 and 350 nm, indicating the presence of different species in equilibrium at the ground state (Figure 1). At pH 9−12, the isosbestic points are observed at 271 and 330 nm.

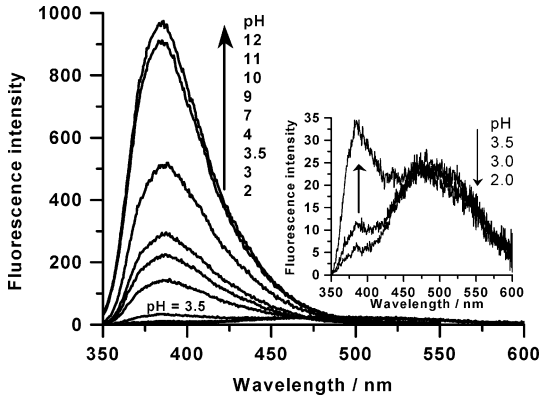

Figure 3. Emission spectra of MIR in aqueous solutions at different pHs upon excitation at 340 nm. The inset shows the emission spectra for pH 2, 3, and 3.5.

At pH ≤3, the spectrum of MIR shows a weak absorption at 266 nm and a stronger and broad band at 325 nm (Figure 2A). Under these conditions, **C** predominates.[9] An increase of pH (4 ≤ pH ≤ 9) leads to an enhancement of the shorter wavelength band intensity and to a shift to longer wavelength (≈13 nm), and narrowing of the longer one (Figure 2). These spectral changes probably reflect the presence of keto−enol tautomeric forms (Figure 1). In neutral buffer solution (pH ∼7) and in pure water, **K** predominates.[2−5] At pH >9, where **A** predominates, the intensity of the longer wavelength absorption band decreases and a red shift to 330 nm is observed, while the shorter wavelength band shows a marked shift ≈14 nm and appears at 280 nm (Figure 2B). The reported pK_a values for MIR are ∼4.5 (pK_{a1}) and ∼8.5 and ∼9.3 (pK_{a2}).[2,3] pK_{a1} represents the deprotonation of the protonated pyridinium moiety (in **C**), whereas pK_{a2} corresponds to deprotonation of neutral structures (Figure 1).[3]

Figure 3 shows the change of emission spectra of MIR at different pH upon excitation at 340 nm. At pH 2, the fluorescence is centered at ∼475 nm, in addition to a very low intensity fluorescence band at ∼385 nm. As the pH increases to 3.5, the intensity of the 385 nm band increases. The excitation spectra gating the two emission bands are different (Figure 4A), indicating that the two fluorescence bands originate from different conformers coexisting at the ground state. The 385-nm fluorescence band is assigned to **K** and the 475-nm band is due to **C**. The delocalization of the positive charge on the pyridinium ring and ICT are responsible for the observed lower energy band of **C** emission (Stokes shift ∼9490 cm^{-1}).

At pH >4.5 (pK_{a1}), MIR exhibits new features. The low-energy fluorescence band due to the emission of **C** is not observed, while the intensity of the higher energy band that corresponds to the emission from **K** increases without any spectral shift. It is worth noting that at neutral pH, i.e. under biologically relevant conditions, where MIR exists as a **K** tautomer (the active species from a pharmacodynamics point of view), the spectrum shows only one emission band. The excitation spectra recorded at two different wavelengths (365 and 440 nm) of observation (Figure 4B) are identical to each

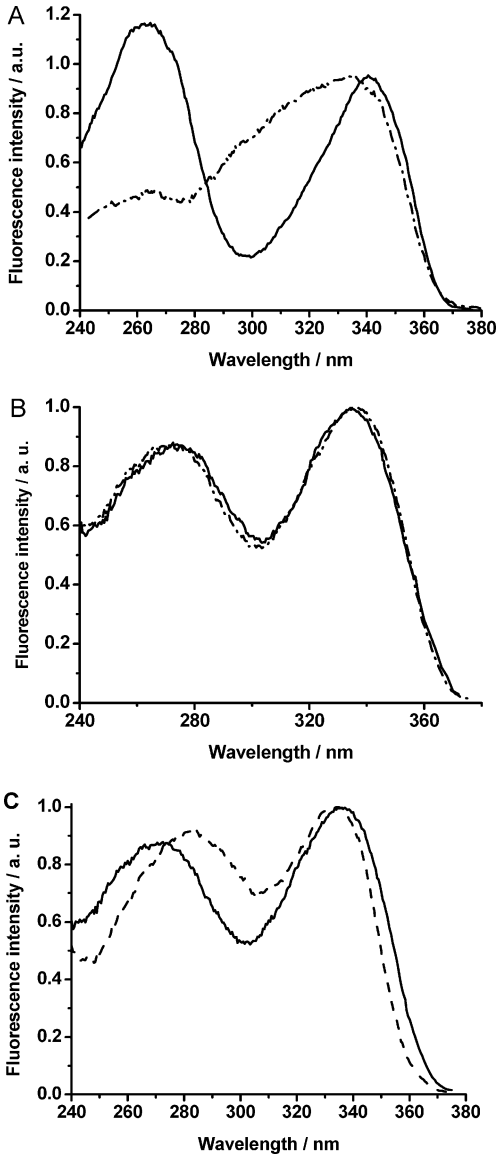

Figure 4. Fluorescence excitation spectra of MIR at different pHs and different wavelengths of observation: (A) pH 3.5 and $\lambda_{obs} = 390$ (—), 480 nm (---); (B) pH 7, $\lambda_{obs} = 365$ (—), 440 nm (---); and (C) pH 7 (—), 12 (---), and $\lambda_{obs} = 390$ nm.

other and not different from the absorption spectrum. This suggests that the observed excited structure originates from only one form (**K** tautomer) at S_0. B3LYP (6-31+G**) calculations showed that in the gas phase, the energy difference between **K** and **E** tautomers is 0.6 kcal/mol, in favor of the former, and their dipole moments are 7.38 and 4.53 D, respectively. In a water cavity, the energy gap increases to 7 kcal/mol, making **K** the most populated structure and the dipole moments become 10.50 and 6.12 D, respectively. The large relative stabilization of **K** in water agrees with the experimental finding.

At pH >9.3 (pK_{a2}), the observed large enhancement of steady-state fluorescence emission (Figure 3) at pH ≈ 11−12 compared to that obtained in acidic or neutral solutions reveals a difference in the nature of the emitting state. The fluorescence excitation spectrum recorded at pH 12 is different from that recorded at pH 7 (Figure 4C). Therefore, at pH 12 the **A** structure becomes the major excited species.

Picosecond Time-Resolved Emission Observation. For a better understanding of the fast interaction of excited MIR in aqueous solutions, we recorded the emission decay at different wavelengths of observation upon excitation at 371 nm. Figure 5 displays representative emission decays of MIR in aqueous solutions of different pH. Table 1 presents the obtained data of the multiexponential fits. We note that although the absorption intensity at 371 nm is very weak, we could observe a reasonable emission signal in time-resolved measurements using picosecond laser excitation and fast detection.

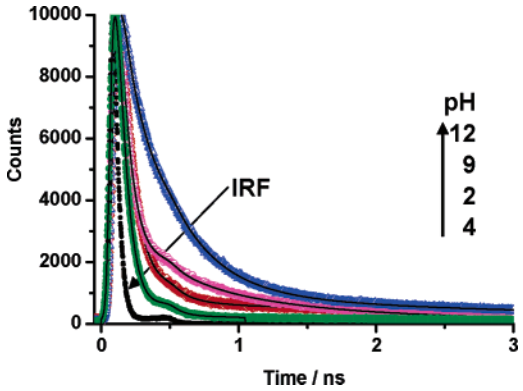

Figure 5. Emission decays (magic angle) of MIR in aqueous solutions at different pH upon picosecond excitation at 371 nm and observation at 480 nm (at pH 2, 4) and 450 nm (at pH 9, 12). The continuous curves are the experimental fit of the data. The IRF signal at ~65 ps is indicated. The extracted data are shown in Table 1.

Table 1. Spectroscopic and Photophysical Data from UV−Visible Absorption and Emission of MIR in Buffer Solutions[a]

pH	λ_{abs}/nm	λ_{em}/nm	λ_{obs}/nm	τ_1/ps	a_1%	τ_2/ps	a_2%	τ_3/ns	a_3%	Φ_f
2.0	266, 325	475	390	92	3	10[b]	97			0.001
			440	95	33	14[b]	66	1.20	1	
			480	90	97			1.48	3	
3.0	266, 325	385, 475	390	90	14	10[b]	86			0.001
			440	90	35	14[b]	64	1.40	1	
			480	90	97			1.43	3	
3.5	266, 325	385, 475	390	63	100					0.003
			440	62	98			1.30	2	
			480	88	97			1.40	3	
4.0	264, 333	385	390	66	100					0.008
			440	68	99			1.38	1	
			480	83	98			1.34	2	
6.0	264, 333	385	390	65	100					0.014
			440	64	99			1.43	1	
			480	68	98			1.40	2	
7.0	264, 333	385	390	69	99			1.23	1	0.015
			440	66	98			1.23	2	
			480	69	98			1.15	2	
9.0	279, 336	385	440	62	87	310	10	1.20	3	0.018
11.0	283, 330	385	440	64	20	307	77	1.30	3	0.065
12.0	283, 330	385	440	62	13	306	85	1.37	2	0.070

[a] The lifetime values (τ_i) and normalized pre-exponential Factors (a_i) upon excitation at 371 nm and the indicated emission wavelengths. [b] <10 ps.

As mentioned above, at pH 2, the emission is mainly from **C**. The fit of the decay recorded at 390 nm is biexponential with time constants of ~90 ps (3%) and <10 ps (97%) (Table 1). When gating the emission at 440 nm, a three-exponential function is necessary to get an accurate fit and gives ~95 ps (33%), <10 ps (66%), and ~1.3 ns (1%). We note that in dioxane, we only observed a picosecond component in the emission decay, which suggests that the nanosecond component found in water is not due to an impurity. At 480 nm, the contribution of the 90-ps component increases to 97%, whereas the shortest (<10 ps) one disappears, making that of the nanosecond component 3%. Thus, we suggest that the 90-ps decay corresponds to the relaxed **C** formed after an ICT2 reaction (Chart 1) in the locally excited (LE) structure, which has the 10-ps component. The nanosecond component is most probably due to deprotonation of the cation, giving **K** and its relaxed form after the production of an ICT2 (see below). This suggestion is supported by its presence in almost all the studied

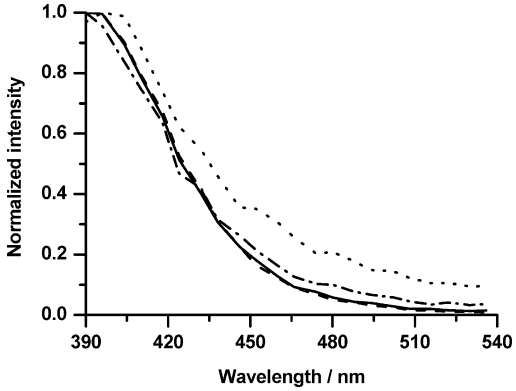

Figure 6. Time-resolved emission spectra (TRES) of MIR in aqueous solution of pH 12 gated at 200 ps (---), 500 ps (—), 1 ns (—·—), and 1.5 (···). The excitation wavelength was 371 nm and IRF ~ 65 ps.

pHs and in other media (vide infra). The ICT in both **C** and **K** takes place in less than 10 ps and could not be detected as a rising component at the blue region. Similar decay features were observed at pH 3. It is worth noting that the **C** form plays an important role in the cardiotonic activity of MIR.[9,25] However at pH 3.5−4, the decay at 390 nm was fitted by one exponential function giving a time constant of ~65 ps, consistent with that obtained in neutral solution where **K** predominates (vide infra). We assign this lifetime to the excited-state **K** tautomer. At longer wavelength of observation (440−480 nm), the decay becomes biexponential and gives the times of relaxed **C** (90 ps, 97%) and relaxed **K** (1.3 ns, 3%).

At 4 < pH < 9, the contribution of **C** emission is insignificant and that of **K** is largely predominant (Figure 3). The time constants of a biexponential fitting are ~65 ps (~98%) and ~1.3 ns (≤2%) due to **K** and its relaxed form (Table 1). The contribution of **K** in the decay is consistent with the excitation spectra in which the main band is due to **K** absorption. Interestingly, the predominance of the **K** tautomer at physiological pH is necessary for positive inotropic activity, therefore increasing the pharmaceutical activity of this cardiotonic drug.[2]

At pH ≥9−12 (pK_{a2}), the decay fit shows three components, indicating the presence of a new species in the relaxation of MIR. At pH ~9, the major contribution (87%) in the emission decreases and is due to **K** (~65 ps), while that of the nanosecond component increases to ~3%. The new component has a time constant of ~310 ps (~10%), and we assign it to **A**. Support for this assignment comes from the pH dependence of the preexponential factor of this component. When we change the pH from 9 to 12, this factor increases from 10 to 85% (Table 1). In this pH range, the **K** component decays with a time constant of 65 ps, but its contribution decreases from 87% at pH 9 to 13% at pH 12. At pH 12, the anionic form (85%) predominates, although the contributions of **K** and nanosecond components are not negligible.

Origin of the Nanosecond Component. We noted that the nanosecond component is observed only at longer wavelengths of emission and over the studied pH range. Figure 6 shows a few time-resolved emission spectra (TRES) of MIR at pH 11 and upon excitation at 371 nm. From the spectral shape change, it is clear that the nanosecond-emission component has its band at the red side of the spectrum. This observation suggests that this component is not due to the **E** form. To gain more insight into the behavior of this nanosecond component, we analyzed the 440-nm fluorescence decay of MIR in tetrahydrofuran (THF), ethylene glycol (EG), and a solid film of poly(methyl methacrylate) (PMMA). For THF we obtained 39 ps (99%) and ~1 ns (1%), and for EG, a ~25 times more viscous solvent,

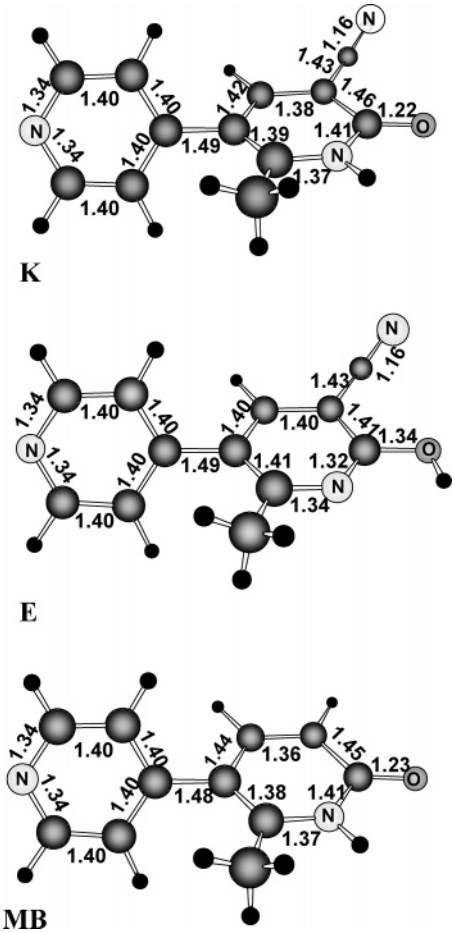

Figure 7. Bond length (in Å) of the optimized structures for the ground state of **K**, **E**, and **K** without the CN group [5-methyl-3,4′-bipyridin-6(1*H*)-one, **MB**] in a water cavity.

we obtained 70 ps (17%), 1.9 ns (7%), and 308 ps (76%). In PMMA rigid matrix, we obtained 5.4 ns (42%), 222 ps (31%), and 1.34 ns (27%). These results show that the contribution of the nanosecond component increases with the viscosity (or rigidity) of the medium. Moreover, upon inclusion of MIR in the cyclodextrin (CD) nanocavity, the contribution of this component weakly increases. For example, in 16 mM β-CD, we observed 61 ps (75%), 235 ps (20%), and 1.6 ns (5%). The results suggest that the species corresponding to the nanosecond component is sensitive to a further twisting motion of the pyridine part. Precluding the pyridine ring rotation increases the lifetime and the contribution of the involved structure in the emission decay, as is actually observed in viscous, rigid, and nanocaging media. The results of the theoretical calculations give other interesting information. The total charges of **K** and **E** of MIR and 5-methyl-3,4′-bipyridin-6(1*H*)-one (**MB**), a molecule with a structure similar to MIR but without the CN group (Figure 7), reveal that, within a water cavity (continuum dielectric model), the Mulliken charge difference between the aromatic moieties is 0.05, 0.05, and 0.006 au for **K**, **E**, and **MB**, respectively. Therefore, the data suggest that at least for the ground state of neutral structures, an ICT reaction does not occur between the aromatic moieties, but it may happen to the CN group (ICT1, Chart 1). In agreement with this later suggestion, the dipole moment value of **MB** (4.1 D) is lower than that of **K** (10.5 D), revealing that the CN group significantly induces an ICT1 process. Moreover, for **K** the calculations show that the Mulliken charge density at the CN group is −0.828 and +0.877 au at the rest of pyridone moiety. This charge difference indicates that the charge transfer takes place from

Table 2. Mean Values of the Photophysical Data of MIR Structures in Water Solutions

structure	τ/ps[a]	Φ_f[b]	$k_r/10^8\ s^{-1}$	$k_{nr}/10^8\ s^{-1}$
keto	65	0.014	2.2 ± 0.6	150 ± 40
cation[c]	90[c]	0.001	0.0012 ± 0.0003	100 ± 30
anion	310	0.047	1.3 ± 0.37	15 ± 4

[a] ±10%. [b] ±20%. [c] Relaxed cation to ICT2.

the pyridone part to the CN group. For **E** structure, the charge density at CN is −0.735 and +0.799 au for the rest of the hydroxy pyridine ring. These values are slightly lower than those calculated for **K**, suggesting relatively less efficient charge-transfer character within **E**. Therefore, the calculations suggested the importance of CN in the stability of the inotropic form (**K**).

The experimental results show that although differences in UV−visible absorption properties were recorded for **A** and **K**, the **A** emission has the same maximum wavelength but a larger intensity with respect to **K** (Table 1 and Figure 3). However, fluorescence excitation spectra recorded at pH 7 and 12 (Figure 4C) and time-resolved data [τ(**A**) = 310 ps and τ(**K**) = 65 ps] indicate a significance difference. We note that because of the limited picosecond time resolution of the used apparatus, we could not observe any rising component that may connect these structures. We are currently exploring the dynamics of MIR in water solution at the femtosecond time scale.

H-Bonding Interaction, Intramolecular Charge Transfer, and Twisting Motion. To get information on the nonradiative rate constant (k_{nr}), we determined the fluorescence quantum yield (Φ_f) values at different pHs (Table 1). At pH 2, **C** predominates and the recorded $\Phi_f \sim 0.001$ is mainly due to relaxed **C**. At pH 6, Φ_f is due to **K**. Because the wavelengths of excitation and emission are fixed in the pH range 9−12, the change in the normalized preexponential factors (a_j) will reflect the relative population changes of the different excited forms. In this case the contribution of individual quantum yields, $\Phi_f(I)$, to the total, $\Phi_f(T)$, can be represented as $\Phi_f(I) = \Phi_f(T)[a_I/\sum_{j=1}^{3} a_j]$, where I represents the excited structures **K**, **A**, or relaxed **C** and T refers to the experimental total quantum yield at any pH. Using this procedure, the calculated Φ_f for **K** is ∼0.015 at pH 9−11. This value is in good agreement with that obtained experimentally (0.014) at pH 6, where **K** predominates (Table 1). The relative contribution of **K** at pH 11−12 is relatively small, so the average of the calculated value $\Phi_f = 0.047$ is due to **A**. Table 2 gives the values of the calculated radiative (k_r) and nonradiative (k_{nr}) rate constants for **A**, **K**, and relaxed **C** in the corresponding water solutions. Figure 8 shows a relative energy diagram and gives emission lifetime and quantum yield values for **C**, **K**, **A**, and charge-transfer species in water solutions. Taking into account the experimental and calculation errors for Φ_f and τ determination, the shortening in the emission lifetime of relaxed forms of **C** and **K** is due to their higher k_{nr} values ($\sim 10^{10}\ s^{-1}$) when compared to that of **A** ($\sim 10^9\ s^{-1}$). In addition to the ICT processes discussed above, other channels might be more efficient in these structures**.** At pH >9, **A** has fewer hydrogen-bonding sites than **K** and **C** formed at lower pH. Since **K** has three hydrogen-bonding sites—NH, C═O, and the nitrogen atom of 3-(4-pyridyl) moiety (Chart 1)—the origin of the deactivation channels could be the formation of an intermolecular hydrogen bond with water molecules in which the H-bond strength changes significantly upon electronic excitation, as has been reported for comparable systems in water.[26,27]

The Stokes shift (energy difference between the maxima of absorption and emission intensity bands) of MIR in neutral water (3750 cm^{-1}) is larger than that recorded in THF (3240 cm^{-1}), and this is generally indicative of a stronger H-bonding interaction with water. However, in THF the observed fluorescence lifetimes are relatively shorter (39 ps and ∼1 ns) than the decay components in water (∼65 ps and 1.3 ns), indicating that efficient fluorescence quenching also occurs in THF. Therefore, further nonradiative channels involving a non-hydrogen-bonding interaction are also efficient for the S_1 relaxation.

The calculations (gas phase) showed that **K** is stabilized under a rotamer conformation in which the C−C bond connecting the two aromatic moieties is twisted by an angle of 51°. For **E** and **MB** structures, the dihedral angle is 53° and 49°, respectively, suggesting that the CN group has an insignificant role in the twisting motion. Results of X-ray crystallography (solid state) and ^{1}H NMR studies (water solution) have revealed that the C−C bond connecting the two aromatic moieties of **K** is twisted

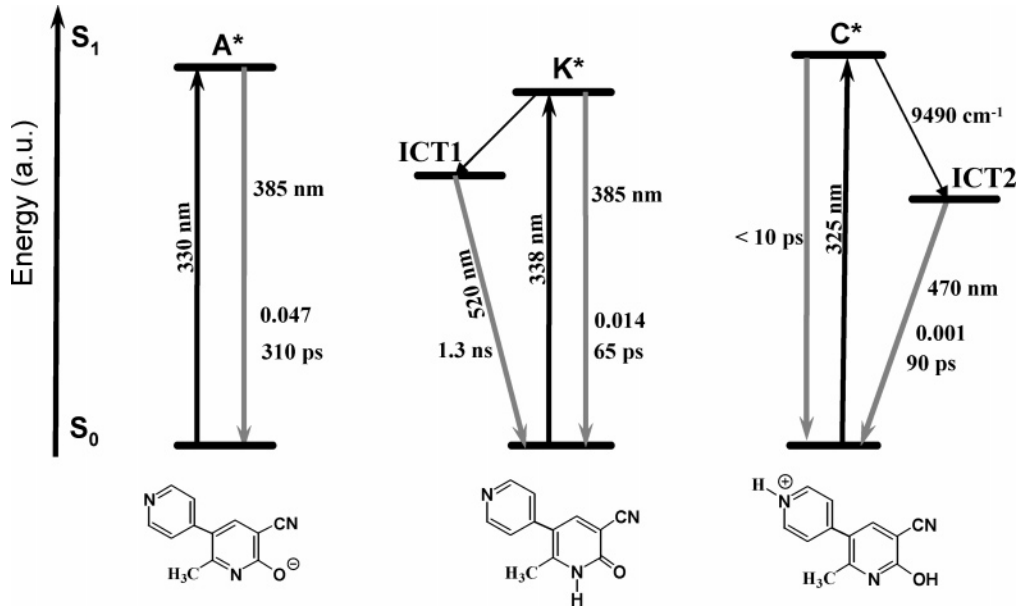

Figure 8. Energy diagram for UV−visible absorption and emission transition of **A**, **K**, and **C** molecular structures of MIR in the corresponding water solution. For simplicity, we referred the S_0 states to the same level for the three structures. ICT1 and ICT2 are the intramolecular-charge-transfer reactions from the pyridine ring to the CN group or pyridine moiety, respectively. The indicated values are of the maximum in intensity of absorption and emission wavelengths (in nm), fluorescence lifetime, and quantum yield.

by 52.2°.[28] However, the ICT2 process and twisting motion might be affected by the presence of the steric effect of the 2-methyl substitutent, thus influencing the dynamics of **K**. It is noteworthy that previous studies of the structure−activity relationship have indicated that the methyl substitutent, rather than the cyano one, is responsible for the inotropic activity of **K**.[3,28]

Laser-induced fluorescence and population-labeling studies of pyridin-2(1*H*)-one led to the conclusion that the structure of **K** has two close lying electronic states in the S_1 region.[29] For MIR, the S_1 (π,π^*) state of **K** may be easily mixed with the close lying (n,π^*) state through vibronic coupling. The efficiency of this coupling might be enhanced by the nonplanarity and twisting motion, leading to further nonradiative deactivation of **K** at the S_1 state. A similar conclusion was reached for 1-methyl-2(1*H*)-pyridinimine.[30] Thus, MIR relaxation in water solutions reflects the interaction with the surrounding molecules involving H-bonding, polarity, and viscosity effects, and the extent of these depends on the pH of the medium. To better understand these interactions, results of picosecond and femtosecond studies of solvent and nanocaging effects will be soon reported.

Conclusion

In this contribution, we attempted to link the features of spectral and excited-state relaxation to the molecular structures of MIR in solution for a better understanding of its interaction with water. The medicine has been found to exist in different structures depending on the pH of the medium. The studies of excited-state relaxation dynamics show short emission lifetime for the highly inotropic active forms **K** (∼65 ps) and **C** (<10 ps). The ICT reactions in these structures give species having emission lifetimes of 1.3 ns and 90 ps, respectively. The lifetime of the inotropic inactive **A** form is 310 ps. The results suggest that H-bonding, twisting motion, and ICT are perhaps key features for inotropic activity of **K** and **C** structures. The calculations at the ground state show that **K** is more stable than **E** by 7 kcal/mol, and their dipole moments are 10.5 and 6.12 D, respectively. We believe that the information discussed here might be relevant to the stability of MIR and therefore to its pharmaceutical use.

Acknowledgment. This work was supported by the "Consejeria de Sanidad" of JCCM and MEC through projects SAN-04-000-00 and SAB2004-0086. M.E. thanks the MEC for the sabbatical year fellowship.

References

(1) Alousi, A.; Canter, J.; Montenaro, M.; Fort, D.; Ferrari, R. Cardiotonic activity of milrinone, a new and potent cardiac bipyridine, on the normal and failing heart of experimental animals. *J. Cardiovasc. Pharmacol.* **1983**, *5*, 792−803.

(2) Altomare, C.; Cellamare, S.; Summo, L.; Fossa, P.; Mosti, L.; Carotti, A. Ionization behavior and tautomerism-dependent lipophilicity of pyridine-2(1*H*)-one cardiotonic agents. *Bioorg. Med. Chem.* **2000**, *8*, 909−916.

(3) de Candia, M.; Fossa, P.; Cellamare, S.; Mosti, K.; Carotti, A.; Altomare, C. Insights into structure−activity relationships from lipophilicity profiles of pyridin-2(1*H*)-one analogs of the cardiotonic agent milrinone. *Eur. J. Pharm. Sci.* **2005**, *26*, 78−86.

(4) Elguero, J.; Marzin, C.; Katritzky, A.; Linda, P. *The Tautomerism of Heterocycles: Supplement 1, Advances in Heterocyclic Chemistry*; Academic: New York, 1976; pp 87−102.

(5) Beak, P.; Covington, J.; White, J. Quantitative model of solvent effects on hydroxypyridine-pyridone and mercaptopyridine-thiopyridone equilibriums: Correlation with reaction-field and hydrogen-bonding effects. *J. Org. Chem.* **1980**, *45*, 1347−1353.

(6) Li, Q.-S.; Fanag, W.-H.; Yu, J.-G. Theoretical studies of proton-transfer reactions of 2-hydroxypyridine-$(H_2O)_n$ (n = 0−2) in the ground and excited states. *J. Phys. Chem. A* **2005**, *109*, 3983−3990.

(7) Karelson, M.; Katritzky, A.; Szafran, M.; Zerner, M. Quantitative predictions of tautomeric equilibria for 2-, 3-, and 4-substituted pyridines in both the gas phase and aqueous solution: Combination of AM1 with reaction field theory. *J. Org. Chem.* **1989**, *54*, 6030−6034.

(8) Cordon, A.; Katritzky, A. R.; Roy, S. K. Tautomeric Pyridines. Part X. Effect of substituents on pyridone−hydroxypyridine equilibria and pyridone basicity. *J. Chem. Soc. B* **1968**, 556−561.

(9) Krauze, A.; Vitolina, R.; Garaliene, V.; Sile, L.; Kluša, V.; Duburs, G. 3,4-*trans*-4-Aryl-3-(1-pyridinio)-1,2,3,4-tetrahydropyridine-6-thiolates−New group of potential cardiotonic drugs. *Eur. J. Med. Chem.* **2005**, *40*, 1163−1167.

(10) Douhal, A. Breaking, making, and twisting of chemical bonds in gas, liquid, and nanocavities. *Acc. Chem. Res.* **2004**, *6*, 349−355.

(11) Fayed, T.; Organero, J. A.; Garcia-Ochoa, I.; Tormo, L.; Douhal, A. Ultrafast twisting motions and intramolecular charge-transfer reaction in a cyanine dye trapped in molecular nanocavities. *Chem. Phys. Lett.* **2002**, *364*, 108−114.

(12) Organero, J. A.; Tormo, L.; Douhal, A. Caging ultrafast proton transfer and twisting motion of 1-hyroxyl-2-acetonaphthone. *Chem. Phys. Lett.* **2002**, *363*, 409−414.

(13) Douhal, A.; Amat-Guerri, F.; Acuña, A. U. Probing nanocavities with proton-transfer fluorescence. *Angew. Chem., Int. Ed. Engl.* **1997**, *36*, 1514−1516.

(14) Zhong, D. P.; Douhal, A.; Zewail, A. H. Femtosecond studies of protein−ligand hydrophobic binding and dynamics: Human serum albumin. *Proc. Natl. Acad. Sci. U.S.A.* **2000**, *97*, 14056−14061.

(15) Douhal, A.; Sanz, M.; Tormo, L. Femtochemistry of orange II in solution and in chemical and biological nanocavities. *Proc. Natl. Acad. Sci. U.S.A.* **2005**, *102*, 18807−18812.

(16) El-Kemary, M.; Rettig, W. Multiple emissions in coumarins with heterocyclic substituents. *Phys. Chem. Chem. Phys.* **2003**, *5*, 5221−5228.

(17) El-Kemary, M. Relaxation pathways of photoexcited non-steroidal anti-inflammatory drugs: Flufenamic and mefenamic acids. *Chem. Phys.* **2003**, *295*, 1−10.

(18) El-Kemary, M.; Douhal, A. Photochemistry and photophysics of cyclodextrin caged drug. *Cyclodextrin materials photochemistry, photophysics and photobiology*; Douhal, A., Ed.; Elsevier: New York, 2006; Chapter 4.

(19) Andrade, S.; Costa, S. Hydrogen bonding effects in the photophysics of a drug, piroxicam, in homogeneous media and dioxane−water mixtures. *Phys. Chem. Chem. Phys.* **1999**, *1*, 4213−4218.

(20) Andrade, S.; Costa, S.; Pansu, R. The influence of water on the photophysical and photochemical properties of Piroxicam in AOT/iso-octane/water reversed micelles. *Photochem. Photobiol.* **2000**, *71*, 405−412.

(21) Bosca, F.; Marín, M. L.; Miranda, M. A. Photoreactivity of the non-steroidal anti-inflammatory 2-arylpropionic acids with photosensitizing side effects. *Photochem. Photobiol.* **2001**, *74*, 637−655.

(22) Becke, A. D. Density-functional thermochemistry. III. The role of exact exchange. *J. Chem. Phys.* **1993**, *98*, 45648−5652.

(23) Lee, C.; Yang, W.; Parr, R. G. Development of the Colle−Salvetti correlation-energy formula into a functional of the electron density. *Phys. Rev. B* **1988**, *37*, 785−789.

(24) Frisch, M. J.; et al. *Gaussian 03*, revision B.05; Gaussian, Inc.: Pittsburgh, PA, 2003.

(25) Nouguchi, A.; Konodo, S.; Kuzuya, M. Quantum chemical study on conformational properties of bipyridine cardiotonics. *Chem. Pharm. Bull.* (*Tokyo*) **1993**, *41*, 1331−1336.

(26) Maris, A.; Ottaviani, P.; Caminati, W. Pure rotational spectrum of 2-pyridone...water and quantum chemical calculations on the tautomeric equilibrium 2-pyridone...water/2-hydroxypyridine...water. *Chem. Phys. Lett.* **2002**, *360*, 155−160.

(27) Organero, J. A.; Douhal, A.; Santos, L.; Martinez-Ataz, E.; Guallar, V.; Moreno, M.; Lluch, J. Proton-transfer reaction in isolated and water-complexed 8-hydroxyimidazo[1,2-*a*]pyridine in the S_0 and S_1 electronic states. A theoretical Study. *J. Phys. Chem. A* **1999**, *103*, 5301−5306.

(28) Robertson, D. W.; Beedle, E. E. Swartzendruber, J. K.; Jones, N. D.; Elzey, T. K.; Kauffman, R. F.; Wilson, H.; Hayes, J. S. Bipyridine cardiotonics: The three-dimensional structures of amirnone and milrinone. *J. Med. Chem.* **1986**, *29*, 635−640.

(29) Matsuda, Y.; Ebata, T.; Mikami, N. Population labeling spectroscopy for the electronic and the vibrational transitions of 2-pyridone and its hydrogen-bonded clusters. *J. Chem. Phys.* **2000**, *113*, 573−580.

(30) Inuzuka, K.; Iwasaki, N.; Fujimoto, A. Considerations on the molecular structures and electronic properties of 1-methyl-2(1*H*)-pyridinimine in the ground and lowest excited singlet states. *Chem. Soc. Jpn. Chem. Indust. Chem. J.* **2001**, *7*, 2001−2007.

JM0600038